PLANETARY GEOPHYSICS

Isotopic evidence of long-lived volcanism on Io

Katherine de Kleer[1]*, Ery C. Hughes[1,2], Francis Nimmo[3], John Eiler[1], Amy E. Hofmann[4], Statia Luszcz-Cook[5,6,7], Kathy Mandt[8]

Jupiter's moon Io hosts extensive volcanism, driven by tidal heating. The isotopic composition of Io's inventory of volatile chemical elements, including sulfur and chlorine, reflects its outgassing and mass-loss history and thus records information about its evolution. We used submillimeter observations of Io's atmosphere to measure sulfur isotopes in gaseous sulfur dioxide and sulfur monoxide, and chlorine isotopes in gaseous sodium chloride and potassium chloride. We find $^{34}S/^{32}S$ = 0.0595 ± 0.0038 (equivalent to $\delta^{34}S$ = +347 ± 86‰), which is highly enriched compared to average Solar System values and indicates that Io has lost 94 to 99% of its available sulfur. Our measurement of $^{37}Cl/^{35}Cl$ = 0.403 ± 0.028 ($\delta^{37}Cl$ = +263 ± 88‰) shows that chlorine is similarly enriched. These results indicate that Io has been volcanically active for most (or all) of its history, with potentially higher outgassing and mass-loss rates at earlier times.

Widespread volcanic activity on Jupiter's moon Io is powered by tidal heating of its interior, which arises from Io's orbital resonance with the neighboring moons Europa and Ganymede. Models of the formation of Jupiter's large moons show that Io, Europa, and Ganymede were probably captured into the resonance during their formation process (*1*, *2*). If so, Io and Europa have experienced strong tidal heating for the entire 4.57–billion year (Gyr) history of the Solar System, implying that Io has been volcanically active (either continuously or cyclically) over the same period (*3*).

Io's current volcanic activity resurfaces the moon at a rate of 0.1 to 1.0 cm year^{-1} (*4*). This has erased all impact craters from its surface (*5*), leaving a geological record of only the most recent million years of its history. However, isotopic abundances could record the history of volcanism on Io: If Io's current rates of mass loss [1000 to 3000 kg s^{-1} (*6*)] and outgassing from its interior to its atmosphere have been sustained for billions of years, its reservoirs of volatile elements should be highly enriched in heavy stable isotopes, because atmospheric escape processes generally favor the loss of lighter isotopes. Stable isotope measurements of volatile elements, such as sulfur and chlorine, could provide information on the history of volcanism on Io.

[1]Division of Geological and Planetary Sciences, California Institute of Technology, Pasadena, CA 91125, USA. [2]Earth Structure and Processes, Te Pū Ao | GNS Science, Avalon 5011, Aotearoa New Zealand. [3]Department of Earth and Planetary Sciences, University of California Santa Cruz, Santa Cruz, CA 95064, USA. [4]Jet Propulsion Laboratory, California Institute of Technology, Pasadena, CA 91109, USA. [5]Liberal Studies, New York University, New York, NY 10023, USA. [6]Columbia Astrophysics Laboratory, Columbia University, New York, NY 10027, USA. [7]Department of Astrophysics, American Museum of Natural History, New York, NY 10024, USA. [8]NASA Goddard Space Flight Center, Greenbelt, MD 20771, USA.
*Corresponding author. Email: dekleer@caltech.edu

Submillimeter observations of Io

We used the Atacama Large Millimeter/submillimeter Array (ALMA) to observe gases in Io's atmosphere (*7*). Io is tidally locked to Jupiter; the hemispheres facing into and away from its direction of motion (its leading and trailing hemispheres) were observed on 2022 May 24 and 2022 May 18, respectively (Universal Time, UT). We used ALMA's Band 8 receivers to cover the frequency range of 416 to 432 GHz (~0.7 mm wavelength) in 13 spectral windows. This frequency range was chosen to cover multiple rotational transitions of SO_2, SO, NaCl, KCl, and their isotopologues, with the goal of determining the $^{34}S/^{32}S$ and $^{37}Cl/^{35}Cl$ ratios. The data were processed (*7*) to produce a calibrated spectral data cube, with dimensions of right ascension (RA), declination (Dec), and frequency, with Io's thermal emission continuum subtracted. The data have a spectral resolution of 244 kHz (170 m s^{-1}) and an angular resolution of ~0.28 arc sec (″) (equivalent to a spatial resolution of ~1000 km at the distance of Io at the time of our observations). The data cubes and extracted images for each species have a pixel scale of 0″.03, such that the spatial resolution is sampled with ~10 pixels per resolution element (*7*).

Figure 1 shows the spatial distribution of each of the four gas species that we targeted. SO_2 and SO are concentrated in the low-to-mid latitudes, with the strongest emission close to the limb, where the atmospheric path length is longest. By contrast, NaCl and KCl are confined to a few localized points, which we interpret as volcanic plumes (locations listed in table S4).

From the data cubes, we extracted disk-integrated spectra around the targeted emission lines (Figs. 2 and 3), using an aperture defined by all pixels in which the continuum emission is at least 5% of the peak continuum emission; this produces an aperture radius that is roughly 1.3× Io's radius. We quantify the noise in the spectrum for each of the 13 spectral windows independently, calculating it as the standard deviation of the disk-integrated spectrum in line-free regions.

Atmospheric modeling

We used a radiative transfer model of Io's tenuous atmosphere (*7*–*9*) to determine the $^{34}S/^{32}S$ ratio, by fitting the observed emission lines of SO_2. SO_2 makes up ~90 to 97% of Io's atmosphere (*10*), so the abundances of all other species in the model are calculated as mixing ratios relative to SO_2. To determine the $^{34}S/^{32}S$ ratio, we jointly fitted two lines of $^{32}SO_2$ and four lines of $^{34}SO_2$. The SO lines were not used in the model fitting, because of the low signal-to-noise ratio (SNR) of the ^{34}SO lines. The free parameters in the model are the SO_2 column density, the $^{34}S/^{32}S$ ratio, and the gas temperature. The gas temperature is constrained because the dataset includes both high- and low-excitation lines. The selection of which $^{34}SO_2$ and $^{32}SO_2$ lines to observe was designed to ensure that they were sensitive to the same altitudes (*7*); therefore, the derived isotopic ratio is not strongly sensitive to the assumed atmospheric temperature profile.

The $^{37}Cl/^{35}Cl$ ratio was determined with the same procedure, by jointly fitting the observed NaCl and KCl lines for both chlorine isotopes (five lines total). The free parameters are the NaCl and KCl column densities (relative to SO_2), the gas temperature, the gas fractional surface coverage (the ratio of the emitting area of the gas to the projected surface area of Io), the $^{37}Cl/^{35}Cl$ ratio, and the line-of-sight gas velocity (relative to Io's velocity and rotation). Gas velocity is a free parameter in the chlorine model because the NaCl and KCl lines are all frequency-shifted from Io's rest frame, with each species shifted in the same way within each observation, indicating bulk motion of the chlorine-bearing gas relative to Io's rotation. This parameter was not necessary for fitting the SO_2 lines.

The observed lines are compared to the best-fitting models in Figs. 2 and 3; the model parameters are listed in Table 1. The SO data are also shown in Fig. 2, which compares them to the model derived from SO_2; we find that the SO data are consistent with the same isotope ratio as derived from SO_2. On Io, SO is produced by photodissociation of SO_2 (*11*), so we expect its $^{34}S/^{32}S$ ratio to only differ from that of SO_2 by a factor of 1.009 (*12*), which is smaller than the uncertainties. The best-fitting SO/SO_2 ratios are 3 and 5% for the leading and trailing hemispheres, respectively, which are within the range of 3 to 10% found by previous studies (*10*, *13*).

The best-fitting gas temperatures for NaCl and KCl (assumed to be identical) are 774 ± 66 and 682 ± 56 K for the leading and trailing hemispheres, respectively (all uncertainties are

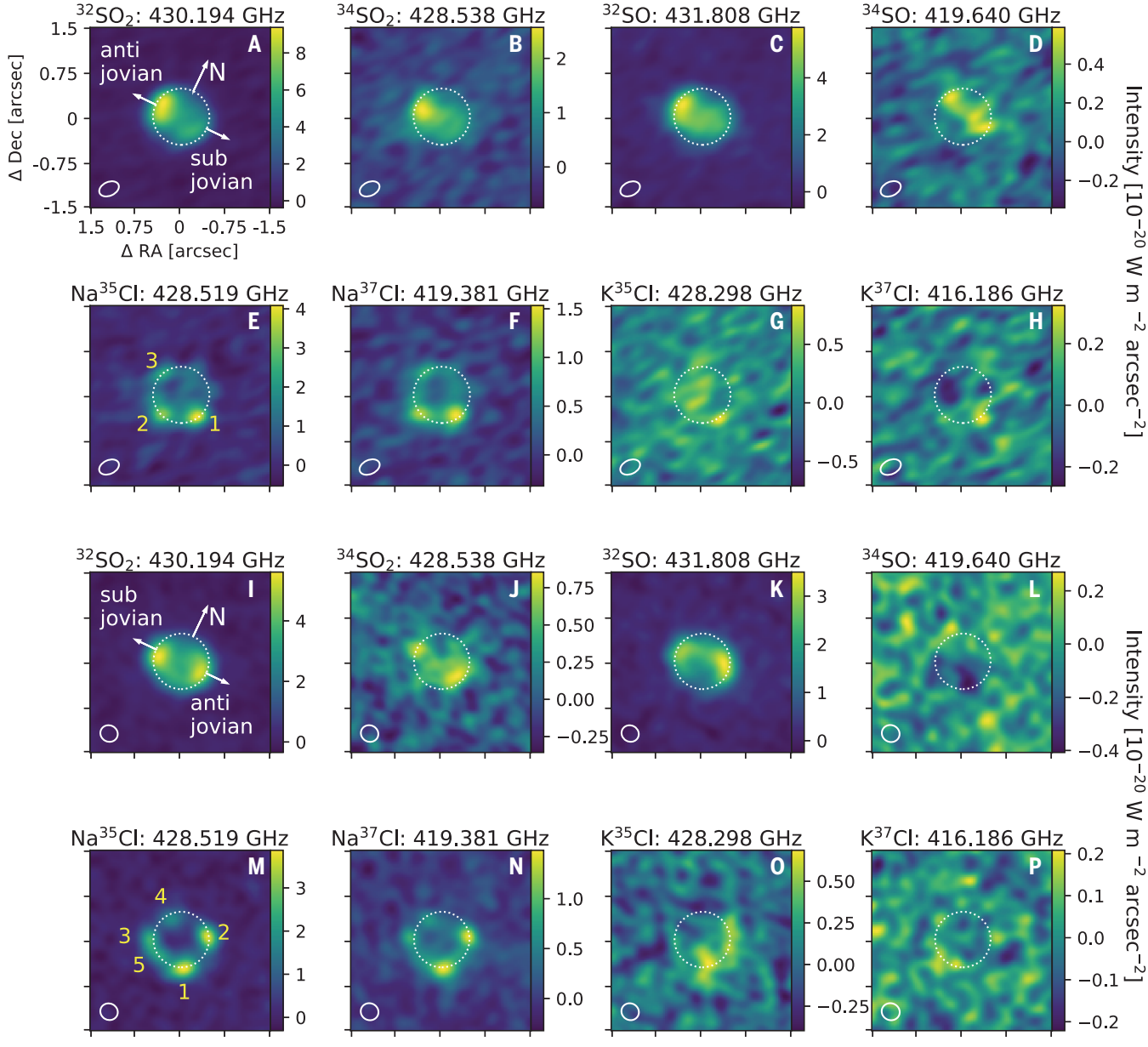

Fig. 1. Observed distributions of molecular emission lines from Io. Each panel shows an image extracted from the ALMA data cube for (**A** to **H**) the leading hemisphere and (**I** to **P**) the trailing hemisphere. For each molecular species (labeled above each panel), we show the strongest detected line, on different intensity scales (color bars). Figures S1 and S2 show equivalent images for all measured lines. The dotted white circles indicate the size and location of Io, and the arrows indicate the north pole, sub-jovian, and anti-jovian directions as labeled. The white ellipses in the lower left corners indicate the size, shape, and orientation of the reconstructed ALMA beam (the spatial resolution). For NaCl and KCl, we interpret the discrete locations of gas emissions as plumes. Specific plumes are numbered in panels (E) and (M); our identifications of the associated surface features are listed in table S4. All panels are on the same angular scale as panel (A), shown as RA and Dec offsets from the center of Io (Δ RA and Δ Dec, respectively).

1σ). These temperatures are consistent with a volcanic plume origin of NaCl and KCl, and within the previously reported range of 500 to 1000 K (*14*). By contrast, the leading and trailing hemisphere temperatures of SO_2, which is present primarily in Io's bulk atmosphere, are 225.9 ± 3.3 and 240.1 ± 7.5 K.

The $^{34}S/^{32}S$ ratio

The leading and trailing hemispheres have $^{34}SO_2/^{32}SO_2$ ratios of 0.0543 ± 0.0022 and 0.0646 ± 0.0053, respectively, a difference of <1.5σ. Combining these, we find a global $^{34}SO_2/^{32}SO_2$ ratio of 0.0595 ± 0.0038. This is less than 2σ below the bottom of the previously reported range of 0.065 to 0.120 (*15*). The previous measurement used $^{32}SO_2$ and $^{34}SO_2$ lines that were sensitive to different altitudes (*7*), so was affected by degeneracies with the temperature profile.

We convert the derived isotope ratio to a $\delta^{34}S_{VCDT}$ value, defined as the difference between the measured value and the Vienna Canyon Diablo Troilite (VCDT) isotopic standard, which has $^{34}S/^{32}S = 0.04416$ (*16*). We find that $\delta^{34}S_{VCDT} = +347 \pm 86$‰ for SO_2 in Io's atmosphere. Figure 4A compares this measurement to other Solar System bodies; we find that Io's atmosphere is more enriched in ^{34}S than most of these materials, by a large margin. The only similarly high enrichment is for H_2S in Comet Hale-Bopp, but that measurement is still consistent with 0‰ (within 2σ), given its large uncertainties (table S5).

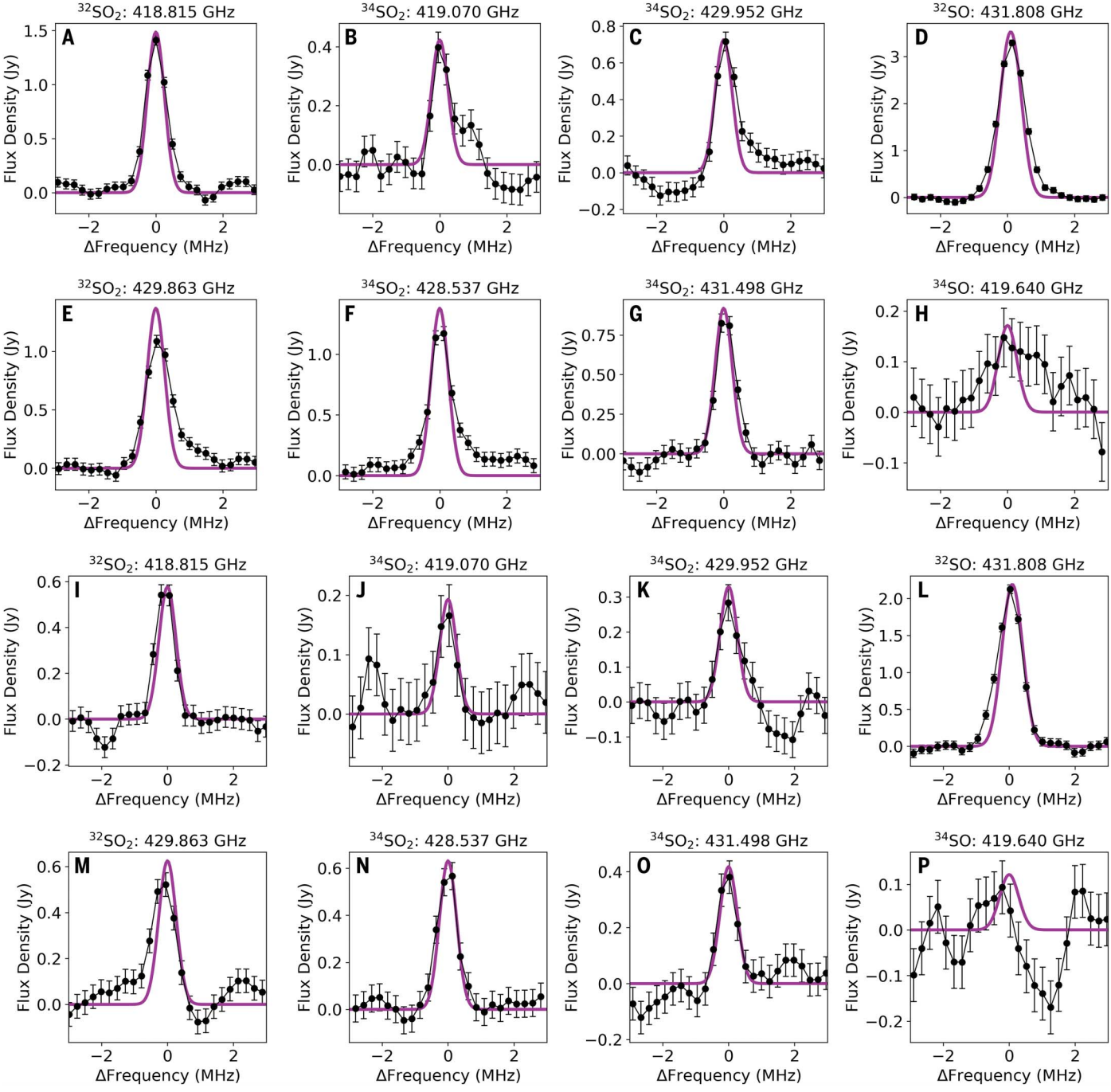

Fig. 2. Spectra of emission lines from the sulfur-bearing molecules. Black points show the measured spectra in janskys (Jy) extracted from the ALMA data cube, integrated over (**A** to **H**) the leading hemisphere and (**I** to **P**) the trailing hemisphere. Eight emission lines are shown, with the species and frequency labeled above each panel. Error bars are 1σ uncertainties. Magenta curves are our best-fitting atmospheric models, fitted to all the lines simultaneously. The best-fitting parameters are listed in Table 1.

We interpret the measured sulfur isotopic fractionation as due to a distillation process, whereby the lighter isotope is preferentially lost from a sulfur reservoir that is being continuously recycled between Io's interior and atmosphere. Atmospheric escape then distills the portion of Io's planetary inventory of sulfur that is available for recycling and loss.

Io's mass loss is driven by ion-neutral collisions between molecules in Io's atmosphere and energetic particles from the plasma in Jupiter's magnetosphere (*17*), not by thermal escape (*18*). Io's atmosphere is thought to be well-mixed up to a boundary known as the homopause [altitude ~30 km (*19*)]. Between the homopause and another boundary known as the exobase (altitude ~600 km), molecular diffusion produces a gravitationally stratified atmosphere (*20*). In the exosphere (above the exobase), the atmosphere is collision-less. Io's mass loss primarily occurs above the exobase, because the conductive ionosphere diverts incoming plasma away from the near-surface region (*21*). From the homopause to the exobase,

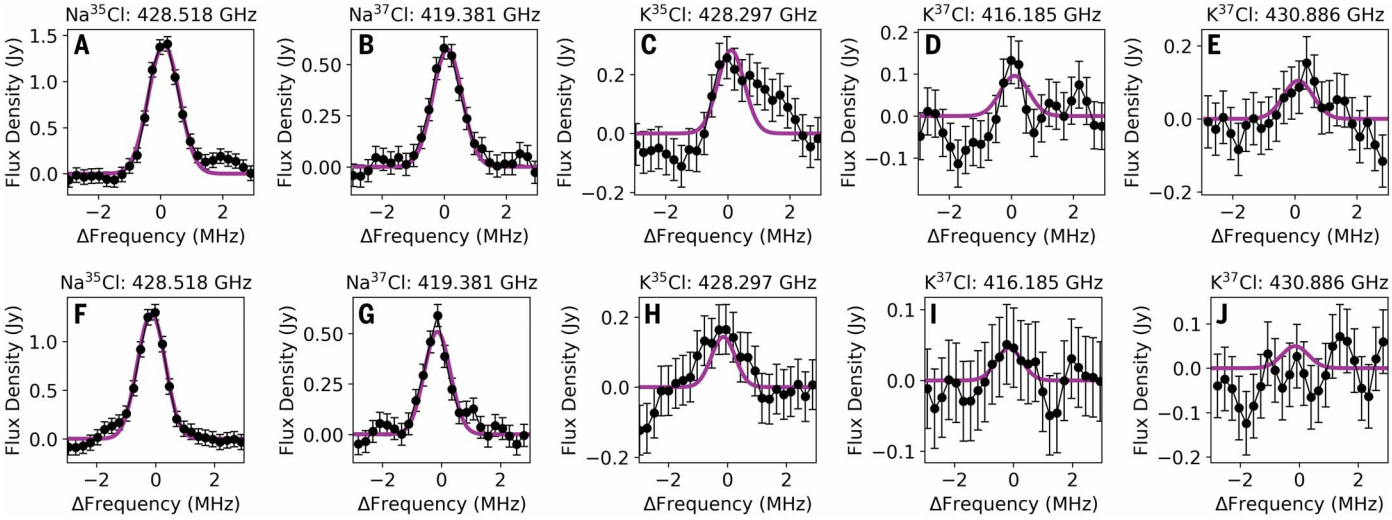

Fig. 3. Same as Fig. 2, but for the chlorine-bearing molecules.

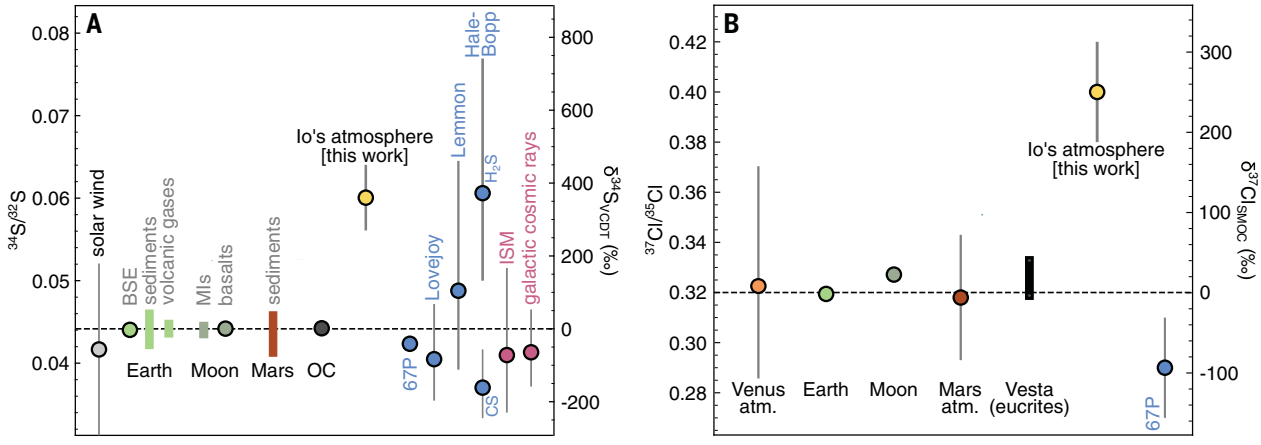

Fig. 4. Isotopic measurements of Io's atmosphere compared to other Solar System bodies. (**A**) Sulfur isotopes, on both the $^{34}S/^{32}S$ (left axis) and $\delta^{34}S_{VCDT}$ (right axis) scales. (**B**) Chlorine isotopes, on the $^{37}Cl/^{35}Cl$ and $\delta^{37}Cl_{SMOC}$ scales. In both panels, circle data points indicate single measurements, whereas rectangular colored bars indicate measurements of a range of samples. The yellow circle is our measurement for Io's atmosphere. Other points show different bodies, including bulk silicate Earth (BSE), lunar melt inclusions (MIs), ordinary chondrite (OC) meteorites, Comet 67P/Churyumov-Gerasimenko (67P), Comet C/2014 Q2 (Lovejoy), Comet C/2012 F6 (Lemmon), the molecules CS and H_2S in Comet Hale-Bopp, the interstellar medium (ISM), the atmospheres (atm.) of Mars and Venus, and eucrite meteorites from Vesta. Points are arranged horizontally in order of the distance of each body from the Sun, not to scale. Data sources are listed in table S5, and error bars show 1σ uncertainties.

the partial pressure of each species decreases as $e^{-mg_z\Delta z/kT_z}$, where m is the mass of the species (in kg mol^{-1}), z is altitude (m), g_z is Io's gravity at that altitude (1.8 m s^{-2} at the surface), k is the Boltzmann constant, and T_z is the gas temperature at that altitude (K).

To determine how isotopically fractionated the material lost from Io's exosphere is, we compare the isotope ratio in SO_2 at the exobase to that at the homopause; for the latter, we assume the isotopic ratio matches that of the well-mixed lower atmosphere. Adopting a temperature profile from previous work (*19*), we calculate that the material lost from Io's atmosphere has a $^{34}S/^{32}S$ ratio 0.917 times that of the bulk atmosphere, which is the loss fractionation factor $^{34}\alpha_{loss}$ (see supplementary text).

If the atmosphere were in steady-state, with mass loss balanced by new material fed from a reservoir with $\delta^{34}S_{VCDT}$ ~0‰ (so with no distillation process), the atmospheric $\delta^{34}S_{VCDT}$ value would be $1 - {}^{34}\alpha_{loss}$ = +83‰. This steady state-value is much lower than the +347 ± 86‰ that we measured, so we reject the possibility of a steady-state system without distillation.

A distillation process, consisting of recycling between the interior and atmosphere combined with mass loss from a gravitationally stratified atmosphere, is consistent with additional constraints on the interactions between Io's surface and interior. If Io has maintained its current resurfacing rate (0.1 to 1.0 cm year^{-1}) over the entire 4.57-Gyr history of the Solar System, and if that resurfacing predominantly occurs through volcanic deposition, then the volume of material required is 10 to 100 times Io's total volume. It is likely that Io's mantle participates in this cycle: Io's magmas are thought to be mantle material melted by tides and advected to the surface through heat pipes (*22*, *23*). Some fraction of the mantle, including its volatile elements, must therefore have been recycled through the surface environment at least tens to hundreds of times.

Table 1. Atmospheric model parameters. The best-fitting model parameters determined from our atmospheric models and the observed molecular emission lines. The models for sulfur- and chlorine-bearing molecules were fitted separately and have different numbers of free parameters. The observations of each hemisphere were also fitted separately. Uncertainties are 1σ (*7*). The column densities of sulfur-bearing molecules assume that the gas is uniformly distributed over Io's surface; if the assumed surface coverage were decreased, the derived column densities would increase proportionally, but other parameters would be unchanged. Similarly, the column densities of the chlorine-bearing molecules are sensitive to the emission angle that is adopted for the model calculation.

Sulfur-bearing molecules

Location	SO_2 column density (cm^{-2})	T_{gas} (K)	$^{34}SO_2/^{32}SO_2$
Leading hemisphere	$(1.029 \pm 0.032) \times 10^{16}$	225.9 ± 3.3	0.0543 ± 0.0022
Trailing hemisphere	$(3.53 \pm 0.21) \times 10^{15}$	240.1 ± 7.5	0.0646 ± 0.0053

Chlorine-bearing molecules

	NaCl column density (cm^{-2})	KCl column density (cm^{-2})	Fractional coverage	T_{gas} (K)	$^{37}Cl/^{35}Cl$	Velocity ($m\ s^{-1}$)
Leading hemisphere	$(5.1 \pm 2.0) \times 10^{13}$	$(9.9 \pm 3.9) \times 10^{12}$	0.133 ± 0.048	774 ± 66	0.415 ± 0.026	75 ± 12
Trailing hemisphere	$(3.3 \pm 1.8) \times 10^{13}$	$(3.5 \pm 2.0) \times 10^{12}$	0.158 ± 0.071	682 ± 56	0.391 ± 0.029	−99.0 ± 5.0

Io's mass-loss history

Assuming that loss from a gravitationally stratified atmosphere is the dominant isotopic fractionation process acting on Io's sulfur inventory, our calculated $^{34}\alpha_{loss}$ relates Io's sulfur isotope ratio today to the fraction of Io's initial sulfur that remains (*f*) via the Rayleigh equation for a constant fractionation factor α:

$$^{34}R = {}^{34}R_0 f^{^{34}\alpha_{loss}-1} \quad (1)$$

where $^{34}R = {}^{34}S/{}^{32}S$, and $^{34}R_0$ is its initial value in bulk Io (see supplementary text). If Io started with $^{34}R_0$ close to the Solar System average ($\delta^{34}S_{VCDT}$ ~0‰, Fig. 4A), our measured isotope ratio corresponds to $f = 0.028^{+0.033}_{-0.015}$, i.e., Io has lost 94 to 99% of its sulfur inventory that participates in the outgassing and recycling process.

In calculating $^{34}\alpha_{loss}$ above, we assumed that loss occurs only above the exobase and that gravitational stratification of the atmosphere is in the steady state. If atmospheric loss also occurs from altitudes below the exobase, or if Io's highly variable atmosphere does not reach a gravitationally stratified steady state, the loss process would produce less isotopic fractionation (higher $^{34}\alpha_{loss}$), so an even greater sulfur fraction would need to have been lost.

We next consider whether the current mass-loss rate, acting on Io's initial sulfur inventory and sustained for 4.57 Gyr, would produce a loss fraction consistent with our measurement. Io is thought to have formed with a bulk composition close to that of ordinary chondrite meteorites classified as types L or LL (*24*), which are ~2% S by mass (*25*). Adopting that composition and Io's current mass gives an estimate of 2×10^{21} kg for Io's initial S mass. At Io's current mass-loss rate of 1000 to 3000 kg s^{-1} (*6*), and assuming that all sulfur loss is through SO_2, Io would have lost (1 to 2) $\times 10^{20}$ kg of S over 4.57 Gyr. This is only 5 to 10% of its initial sulfur inventory, much lower than our calculation of 94 to 99% sulfur loss. We consider several interpretations of this difference.

It is possible that Io's initial sulfur inventory was smaller than our estimate above, for example, if Io formed with lower sulfur abundance than the L/LL chondrites. However, if Io's initial sulfur abundance was instead closer to the Solar System average than to ordinary chondrites (*26*), it would contain more sulfur not less. Io might also have lost a substantial fraction of its initial sulfur content soon after formation (*27*), leaving a smaller effective reservoir for its subsequent mass loss. Another possibility is that the initial $^{34}S/^{32}S$ ratio of Io was higher than the Solar System average. The sulfur in L/LL chondrites has $\delta^{34}S_{VCDT}$ = −0.02 ± 0.06‰ (*28*), consistent with the Solar System average. The most isotopically fractionated sulfur reservoirs across Earth, the Moon, Mars, and meteorites are tens of per mille (Fig. 4A), which is an order of magnitude less fractionated than our measurement of SO_2 in Io's atmosphere. The only ^{34}S measurements for outer Solar System material are for comets. The most precise cometary measurement was made in situ by the Rosetta spacecraft and showed that Comet 67P/Churyumov–Gerasimenko is depleted in the heavy isotope in all sulfur-bearing species (*29*). If some of Io's sulfur came from cometary material, its initial $\delta^{34}S_{VCDT}$ would be lower than Solar System average, not higher. We therefore consider it unlikely that Io had an initial $^{34}S/^{32}S$ ratio that was much higher than the Solar System average.

Alternatively, only a fraction of the sulfur in Io might participate in the mixing and loss cycle, particularly if sulfur is concentrated in the moon's core. Io's mean density and moment of inertia indicate the presence of a core with possible compositions that range from pure Fe to an Fe-FeS eutectic mixture [which is ~25% sulfur by mass (*30*)]. These constraints, combined with experiments on equilibrium sulfur partitioning between metal and silicates, indicate that 80 to 97% of Io's initial sulfur inventory is in the core (*20*). Our measurement of 94 to 99% sulfur loss is therefore consistent with the fraction of noncore sulfur lost if Io has been losing mass at ~0.5 to 5 times its current rate over its entire 4.57-Gyr lifetime. This implies that Io's mass-loss rate could have been higher in the past than it is today.

The $^{37}Cl/^{35}Cl$ ratio

Combining the NaCl and KCl results from both hemispheres (Table 1) gives a $^{37}Cl/^{35}Cl$ ratio of 0.403 ± 0.028. This value is dominated by the NaCl lines, which have much higher SNR than the KCl lines. Similarly to sulfur, we convert this ratio to a $\delta^{37}Cl_{SMOC}$ value, defined as the deviation from the Earth isotopic standard, standard mean ocean chloride (SMOC), which has $^{37}Cl/^{35}Cl = 0.320$ (*31*). We find that $\delta^{37}Cl_{SMOC}$ = +263 ± 88‰ for Io, which is compared to other Solar System reservoirs in Fig. 4B. Chlorine participates in an outgassing and recycling process analogous to that of sulfur, being lost by plasma interactions at a rate of a few percent of that of sulfur (*32*). However, the $^{37}Cl/^{35}Cl$ loss fractionation factor ($^{37}\alpha_{loss}$) is more uncertain than that of sulfur. NaCl and KCl gases in Io's atmosphere are not replenished by sublimation and are destroyed by photodissociation within a few hours of entering the atmosphere (*33*, *34*). Their gas temperatures are high, as discussed above, and their gas dynamics appear to be dominated by volcanic plume processes. We therefore do not expect steady-state gravitational stratification for these molecules, so $^{37}\alpha_{loss}$ should be closer to 1 than $^{34}\alpha_{loss}$. Applying the same distillation reasoning as for sulfur, this leads to the conclusion that $\delta^{37}Cl_{SMOC}$

would be lower than $\delta^{34}S_{VCDT}$ for the same fractional loss. Our measured value of $\delta^{37}Cl_{SMOC}$ therefore also indicates a history of mixing and mass loss, supporting our interpretation of the $\delta^{34}S_{VCDT}$ measurement.

REFERENCES AND NOTES

1. S. J. Peale, M. H. Lee, *Science* **298**, 593–597 (2002).
2. K. Batygin, A. Morbidelli, *Astrophys. J.* **894**, 143 (2020).
3. H. Hussmann, T. Spohn, *Icarus* **171**, 391–410 (2004).
4. C. B. Phillips, *Voyager and Galileo SSI Views of Volcanic Resurfacing on Io and the Search for Geologic Activity on Europa,* thesis (The University of Arizona, 2000); https://repository.arizona.edu/handle/10150/289119.
5. T. V. Johnson, A. F. CookII, I. I. C. Sagan, L. A. Soderblom, *Nature* **280**, 746–750 (1979).
6. V. Dols, P. A. Delamere, F. Bagenal, *J. Geophys. Res.* **113**, A09208 (2008).
7. Materials and methods are available as supplementary materials.
8. S. Luszcz-Cook, K. de Kleer, kdekleer/Io_mm_RT: Code version for models published in de Kleer *et al*., Zenodo (2024);
9. I. de Pater *et al*., *Planet. Sci. J.* **1**, 60–85 (2020).
10. E. Lellouch *et al*., *Astrophys. J.* **459**, L107–L110 (1996).
11. M. E. Summers, D. F. Strobel, *Icarus* **120**, 290–316 (1996).
12. Y. Endo, Y. Sekine, Y. Ueno, *Chem. Geol.* **609**, 121064 (2022).
13. A. Moullet, M. A. Gurwell, E. Lellouch, R. Moreno, *Icarus* **208**, 353–365 (2010).
14. E. Redwing *et al*., *Planet. Sci. J.* **3**, 238 (2022).
15. A. Moullet *et al*., *Astrophys. J.* **776**, 32 (2013).
16. T. Ding *et al*., *Geochim. Cosmochim. Acta* **65**, 2433–2437 (2001).
17. F. Bagenal, V. Dols, *J. Geophys. Res. Space Phys.* **125**, e27485 (2020).
18. E. M. Sieveka, R. E. Johnson, *Astrophys. J.* **287**, 418–426 (1984).
19. J. I. Moses, M. Y. Zolotov, B. Fegley, *Icarus* **156**, 76–106 (2002).
20. E. Hughes, K. de Kleer, J. Eiler, *et al*, *JGR Planets* 10.1029/2023JE008086 (2024).
21. J. Saur, F. M. Neubauer, D. F. Strobel, M. E. Summers, *J. Geophys. Res.* **104**, 25105–25126 (1999).
22. S. J. Peale, P. Cassen, R. T. Reynolds, *Science* **203**, 892–894 (1979).
23. T. C. O'Reilly, G. F. Davies, *Geophys. Res. Lett.* **8**, 313–316 (1981).
24. O. L. Kuskov, V. A. Kronrod, *Icarus* **151**, 204–227 (2001).
25. G. Dreibus, H. Palme, B. Spettel, J. Zipfel, H. Wanke, *Meteoritics* **30**, 439–445 (1995).
26. W. B. McKinnon, "Formation and early evolution of Io" in *Io After Galileo*, R. M. C. Lopes, J. R. Spencer, Eds. (Springer-Praxis Books, 2007), pp. 61–88.
27. C. J. Bierson, F. Nimmo, *Astrophys. J. Lett.* **897**, L43 (2020).
28. X. Gao, M. H. Thiemens, *Geochim. Cosmochim. Acta* **57**, 3171–3176 (1993).
29. U. Calmonte *et al*., *Mon. Not. R. Astron. Soc.* **469** (Suppl_2), S787–S803 (2017).
30. J. D. Anderson, R. A. Jacobson, E. L. Lau, W. B. Moore, G. Schubert, *J. Geophys. Res.* **106**, 32963–32969 (2001).
31. A. Godon *et al*., *Chem. Geol.* **207**, 1–12 (2004).
32. M. Küppers, N. M. Schneider, *Geophys. Res. Lett.* **27**, 513–516 (2000).
33. C. T. Ewing, K. H. Stern, *J. Phys. Chem.* **78**, 1998–2005 (1974).
34. J. I. Moses, M. Y. Zolotov, B. Fegley, *Icarus* **156**, 107–135 (2002).

ACKNOWLEDGMENTS

We thank A. Moullet for insight into past observations of Io, and A. Thelen for help with CASA imaging. We acknowledge the support of R. Loomis, A. Remijan, and the North America ALMA Science Center (NAASC) in obtaining these data and processing them into calibrated images. This project concept was developed in part at the W. M. Keck Institute for Space Studies. ALMA is a partnership of ESO (representing its member states), NSF (USA), and NINS (Japan), together with NRC (Canada), MOST and ASIAA (Taiwan), and KASI (Republic of Korea), in cooperation with the Republic of Chile. The Joint ALMA Observatory is operated by ESO, AUI-NRAO, and NAOJ. The National Radio Astronomy Observatory is a facility of the National Science Foundation operated under cooperative agreement by Associated Universities, Inc. The Jet Propulsion Laboratory (JPL) is operated by the California Institute of Technology under contract with the National Aeronautics and Space Administration (80NM0018D0004). **Funding:** K.d.K. acknowledges funding from National Science Foundation grant 2238344 through the Faculty Early Career Development Program. K.d.K., J.E., E.C.H., and A.E.H. acknowledge funding from the Caltech Center for Comparative Planetary Evolution. K.M. acknowledges support from NASA ROSES Rosetta Data Analysis Program grant 80NSSC19K1306. A.E.H. acknowledges support from the JPL Researchers on Campus Program and from internal JPL funding. K.d.K. acknowledges support from the NAASC through their funding of a PI face-to-face data reduction visit.
Author contributions: K.d.K. led the conceptualization, methodology development, analysis, interpretation, and writing of the manuscript. F.N., J.E., and K.M. contributed to project conceptualization and to development of the Rayleigh distillation model. A.E.H. and E.C.H. contributed to development of the Rayleigh distillation model. S.L.-C. developed the radiative transfer model with contributions from K.d.K. All authors contributed to the interpretation, discussed the results, and revised the manuscript.
Competing interests: The authors declare that they have no competing interests. **Data and materials availability:** This paper makes use of the following ALMA data: ADS/JAO.ALMA#2021.1.00849.S, which are archived at https://almascience.nrao.edu/aq/?projectCode=2021.1.00849.S. The radiative-transfer modeling software is archived at Zenodo (*8*). Our measured atmospheric parameters are listed in Table 1 and table S3.

SUPPLEMENTARY MATERIALS

science.org/doi/10.1126/science.adj0625
Materials and Methods
Supplementary Text
Figs. S1 to S6
Tables S1 to S5
References (*35*–*79*)

Submitted 25 June 2023; accepted 13 March 2024
Published online 18 April 2024
10.1126/science.adj0625